NeuroImage 190 (2019) 303–312

Contents lists available at ScienceDirect

NeuroImage

journal homepage: www.elsevier.com/locate/neuroimage

Decoding neuropathic pain severity using distinct patterns of corticolimbic metabotropic glutamate receptor 5

Geehoon Chung [a,b], Chae Young Kim [a,c], Sang Jeong Kim [a,b,c,d,*]

[a] Department of Physiology, Seoul National University College of Medicine, Seoul, 03080, South Korea
[b] Department of Brain and Cognitive Sciences, Seoul National University College of Natural Sciences, Seoul, 03080, South Korea
[c] Department of Biomedical Sciences, Seoul National University College of Medicine, Seoul, 03080, South Korea
[d] Neuroscience Research Institute, Seoul National University College of Medicine, Seoul, 03080, South Korea

ARTICLE INFO

Keywords:
Neuropathic pain
Positron emission tomography
Metabotropic glutamate receptor 5
[11C] ABP688
Disease marker
Assessment of pain degree

ABSTRACT

Susceptibility to neuropathic pain and the degree of pain amplification vary among individuals. However, methods for objective evaluation of pain status have not been well established. Using an animal model, we identified the brain signature of neuropathic pain, and developed a method for the objective evaluation of pain degree. We analyzed paw withdrawal thresholds from rats that were subjected to right L5 spinal nerve ligation (SNL) surgery, and regressed them to the metabotropic glutamate receptor 5 (mGluR5) availability levels in the brain using [11C] ABP688 PET image data from our previous research. We found clusters with a significant correlation to paw withdrawal threshold localized in brain areas involved in sensory, cognitive, and affective aspects of pain processing. Strikingly, mGluR5 availability levels in the identified brain regions showed distinct patterns in the neuropathic pain group but not in the control group. We successfully elucidated the degree of pain-sensing behavior using the neuropathic pain-specific pattern of the mGluR5 availability. Our study provides new insight into the signature of neuropathic pain in the brain, and offers a novel diagnostic method for objectively decoding the status of individual neuropathic pain.

1. Introduction

Once neuropathic pain is established, patients perceive normally innocuous external sensory stimuli as noxious, and suffer from intractable pain. For many patients, neuropathic pain symptoms are not treatable with conventional methods, and the direct cause of neuropathic pain cannot be identified even with close examination (Singleton, 2005; van Wilgen and Keizer, 2012). Moreover, there is currently no established standard method for objective assessment of pain status (Hu and Iannetti, 2016; Wager et al., 2013), although studies on neuropathic pain have been actively conducted over the past decades. The existing assessment tools primarily rely on the subjective self-report of the patients. In that, it is hard to distinguish false reports, and the methods can not be applied to patients who can not communicate verbally. The lack of the objective method can cause issues on the insurance application and high medical costs due to a communication issue with patients. The manifestation of chronic pain symptoms after nerve injury and the degree of pain experienced vary among individuals (Baron et al., 2012; von Hehn et al., 2012), making it difficult to identify common circuits and develop standard evaluation methods.

Research in humans with neuropathic pain is difficult because of the variation in symptoms and degree of pain as well as psychosocial effects (Baron et al., 2012; Bouhassira and Attal, 2016; Fitzgerald and McKelvey, 2016; Tran et al., 2016; Vase et al., 2016). Therefore, identifying factors that determine the pain behavior in the rodent model is advantageous for understanding mechanisms of neuropathic pain. Various animal models have been developed and studied to clarify mechanisms underlying abnormal sensory processing in the nervous system of patients with neuropathic pain (Kim et al., 1997; Yalcin et al., 2014). In many rodent models of neuropathic pain, mononeuropathy is surgically induced by unilaterally injuring the nerve innervating a hind paw. In such models, evaluation of the paw withdrawal response using the von Frey test is the most commonly applied method for assessing resulting tactile mechanical allodynia (Chaplan et al., 1994; Detloff et al., 2010). When successful, surgically induced neuropathic pain reduces the tactile threshold and evokes sensitized withdrawal behavior in response to a mechanical stimulus applied to the affected paw.

Interestingly, the degree of reduction in paw withdrawal threshold

* Corresponding author. Seoul National University College of Medicine, Research building 701, 103 Daehak-ro, Jongro-gu, Seoul, 03080, South Korea.
E-mail addresses: geehoon.chung@brain.snu.ac.kr (G. Chung), kimcy87@gmail.com (C.Y. Kim), sangjkim@snu.ac.kr (S.J. Kim).

https://doi.org/10.1016/j.neuroimage.2018.07.016
Received 5 April 2018; Received in revised form 8 June 2018; Accepted 6 July 2018
Available online 7 July 2018

following neuropathic pain modeling varies among individual animals, despite being subjected to the same surgical procedures and experimental environment, and being of the same genetic background (Hogan et al., 2004). Reduction of the paw withdrawal threshold involves supraspinal as well as spinal mechanisms (Detloff et al., 2010; Ossipov et al., 2000; Saadé et al., 2006), and the stochastic neural responses to an aberrant pain signal in the circuits are thought to underlie such variation. Previous studies have revealed various neural factors that correlate with paw withdrawal thresholds in animal models of neuropathic and inflammatory pain (Baliki et al., 2014; Coffeen et al., 2010; Kras et al., 2014; Massart et al., 2016; Wei et al., 2017). For example, changes in the functional connectivity between limbic system and sensorimotor cortices (Baliki et al., 2014), the dopamine release in the insular cortex (Coffeen et al., 2010), and the DNA methylation states in the prefrontal cortex (Massart et al., 2016) are correlated with the degree of the paw withdrawal behavior in pain animals. These studies demonstrated that the changes in the brain, as well as in the spinal cord, strongly correlate with the execution of pain behaviors.

Recent neuroimaging techniques have provided a strong foundation for the study of the functional relationship between brain parameters and animal behavior (Litaudon et al., 2017). The significance of higher cortical functions in pain behavior has been the subject of much attention based on observations from clinical studies (Baliki et al., 2014; Roy et al., 2014; Vachon-Presseau et al., 2016; Wager et al., 2013). Indeed, neuroimaging studies of animal models of neuropathic pain and human patients with chronic pain emphasize the critical role of corticolimbic structures of the brain in accounting for the probability, severity, and duration of pain symptoms, independently from spinal level mechanisms (Baliki et al., 2014, 2012; Baliki and Apkarian, 2015; Davis et al., 2016; Vachon-Presseau et al., 2016).

In this study, we focused on the metabotropic glutamate receptor 5 (mGluR5), a key player in the modulation of the neural transmission in the brain. The mGluR5 plays a significant role in information processing and plastic change of neurons, and thus the mGluR5 availability in various brain regions are critically involved in the physiological functions and pathological alterations of the brain circuitry, including amplified pain perception and deciding behavioral coping strategy. Our primary hypothesis was that the sensitized paw withdrawal behavior observed during neuropathic pain is tightly connected to mGluR5 availability levels in sensory and limbic brain structures. We analyzed brain images of animal models of neuropathic pain using positron emission tomography (PET) with mGluR5-specific radiotracer [11C] ABP688 from our previous study (Chung et al., 2017). Strikingly, mGluR5 availability levels showed distinct regional patterns in the brain of neuropathic rats but not control rats. Further, we show that the withdrawal threshold of the individual neuropathic pain subject could be successfully determined from an [11C] ABP688 PET image using this pattern.

2. Material and methods

2.1. Animal experiments

All the experimental procedures were approved by the Institutional Animal Care and Use Committee at Seoul National University and were performed according to the Ethical Guidelines of the International Association for the Study of Pain.

8-week-old male Sprague-Dawley rats (Samtako, Seoul, Korea) were subjected to right L5 spinal nerve ligation (SNL) surgery (Kim and Chung, 1992) or sham surgery under isoflurane anesthesia. In SNL surgery, the right L5 spinal nerve was isolated and tightly ligated using 5-0 silk to induce neuropathic pain. In sham surgery, the L5 spinal nerve was isolated but not ligated. Paw withdrawal thresholds of the affected right hind paw were measured one day before and 1, 5, 9, and 15 days after the surgery. A series of von Frey filaments with logarithmic incremental forces (3.61, 3.84, 4.08, 4.31, 4.56, 4.93, 5.18) were used with Dixon's up-down method and Chaplan's calculation method (Chaplan et al., 1994; Dixon, 1965) to assess 50% paw withdrawal threshold. The withdrawal threshold of 15 g was applied as the cut-off threshold. Animals with abnormal motor deficiency (foot-drop) after the surgery were excluded from analyses. Animals exhibiting sensitive hind paws pre-surgery (paw withdrawal threshold < 10 g) or weak sensitivity post-SNL surgery (paw withdrawal threshold > 5 g) were not considered as the subject of the PET scan, although they underwent behavioral tests during the observation period.

2.2. PET imaging and data processing

The PET images used in this study are from our previous research, and detailed procedures for PET scan and preprocessing of the data are described elsewhere (Chung et al., 2017). Briefly, animals were anesthetized with isofluorane and received a tail vein injection of [11C] ABP688 (5.05–16.15 MBq/100 g). Brain images were acquired using a micro-PET/CT scanner (eXplore VISTA, GE Healthcare) with list-mode for 60 min. The data were reconstructed into a single static image of the full 60 min scan as well as separated binned images of 6 * 30 s, 7 * 60 s, and 5 * 600 s duration, using 3-dimensional OSEM algorithm with scatter correction and random correction. Voxel size was 0.3875 * 0.3875 * 0.775 mm. Each image was reconstructed in proportion to standardized uptake value (SUV). Static images of the full 60 min were coregistered with a standard rat MRI template (Schweinhardt et al., 2003) and the transformation parameters were applied to the respective binned images of each dataset. The non-displaceable binding potential (BP_{ND}) of [11C] ABP688 was calculated using the simplified reference tissue model with the cerebellum as a reference region. The brain mGluR5 template image was made by averaging all the [11C] ABP688 BP_{ND} images, and then all the BP_{ND} images were spatially normalized to this brain mGluR5 template image. Voxels were resampled to 0.2 * 0.2 * 0.2 mm and smoothed with a Gaussian filter of 0.8 mm full-width at half maximum. Images were processed using SPM8, MarsBaR toolbox, and imgsrtm program of Turku PET Centre. Images were acquired between the 16th and the 25th day after the surgery.

2.3. SPM analysis

To investigate the interaction between the mGluR5 availability level in the brain and paw withdrawal threshold, a voxel-wise regression analysis was used with data from SNL group animals. An uncorrected p-value threshold of 0.005 and an extent threshold of 20 voxels were used to screen ROIs. In addition, we reported clusters that survived a threshold of $p < 0.005$ and $p < 0.001$ with permutation-based analyses. Threshold-free cluster enhancement (TFCE) was used with 5000 permutations. The statistical map was overlaid onto an MRI template image (Schweinhardt et al., 2003). For posthoc analyses, region-of-interest (ROI) was set based on the anatomical location of the significant cluster, and BP_{ND} in the 0.5 mm radius sphere of the ROI was extracted using the MarsBaR toolbox (Brett et al., 2002).

2.4. Statistical analysis

Pearson's correlation coefficient method was also used to compute the correlation between the ROIs. The mGluR5 availability levels of each ROI in the SNL group and the sham group were compared using the two-sample *t*-test and F-test.

2.5. Creating a representative template of the mGluR5 patterns

For normalization, the mGluR5 availability levels in each ROIs were separately divided by the average values of each ROIs of the sham group. The normalized values of SNL rats were then regressed to the paw withdrawal thresholds. The regressed values of each ROIs were then plotted in separate columns. As such, a row of regressed mGluR5

templates represents an ideal mGluR5 pattern of a hypothetical SNL rat that has a corresponding paw withdrawal threshold.

2.6. Deciphering the pain status using the mGluR5 patterns

A normalized mGluR5 pattern of a rat was applied to the regressed template row-by-row, to calculate Pearson's correlation coefficients. The calculations were repeated for all rats, and the results for each rat were plotted to the separated columns. Thus, each column of the r-value and p-value matrices represents the result from an individual rat.

2.7. Cross-validation

The sensitivity of the method was investigated using leave-one-subject-out cross-validation. In this paradigm, the data of one subject was left out after the ROI selection or before the ROI selection. In the former case, the pattern data of one subject (mGluR5 availability levels in 12 ROIs) were left out, and the regressed template was created from data of the remaining nine subjects. Then, data of the subject that had been left out (the mGluR5 availability data from 12 ROIs) were applied to the regressed template row-by-row, to calculate the correlation coefficients. This method was repeated subject-by-subject to predict all the paw withdrawal thresholds of SNL subjects. In the latter, additional cross-validation test, the data of one subject (test sample subject) was left out before the ROI selection, and the following procedure was performed. Depending on the trials, 9 to 17 ROIs were selected based on the PET images from the remaining nine subjects. The mGluR5 availability levels were extracted from the ROIs of the corresponding trial. The regressed template was created using data from the nine subjects with the corresponding ROI set. Then the pattern data from the subject which had been left out (the pattern data of the test sample subject with the trial-specific ROI set) were applied to the regressed template row-by-row to calculate the correlation coefficients. The tests were repeated subject-by-subject.

3. Results

3.1. Variation of the paw withdrawal threshold following nerve injury-induced neuropathic pain

We adopted the data from 103 rats that were subjected to right L5 SNL surgery during the study period of our previous research (Chung et al., 2017). The paw withdrawal threshold was successfully and persistently reduced after the SNL surgery in the majority of subjects (Fig. S1A). As previously described, there was some variation in the degree of behavioral responses of the animal models of neuropathic pain, despite being subjected to identical procedures (Hogan et al., 2004). Consistent with previous studies, paw withdrawal thresholds were distributed with positive skew (Fig. S1B), and in approximately 15% of animals (14 out of 103 rats), the threshold was merely reduced (>50% of baseline threshold) despite SNL surgery. This ratio is in agreement with reports of SNL surgery in the same rodent-strain of ours (Sprague-Dawley rats) (Felice et al., 2011). We focused on the brains of animals that demonstrated successful induction of neuropathic pain; non-allodynic animals did not undergo [11C] ABP688-PET scan. Rats with appropriately non-sensitive hind paw response during baseline measurement (paw withdrawal threshold > 10 g) and successful induction of mechanical allodynia were subjected to PET scan (n = 10 SNL rats; Fig. S1, B and C, red data points). We further confirmed that the observed variation was common across the 31 surgery batches performed during the research period (Fig. S1C).

3.2. Brain regions in which mGluR5 availability is correlated to behavioral response

Using a regression analysis of the [11C] ABP688-PET images from this group, we investigated the brain regions in which mGluR5 availability levels are tightly connected to paw withdrawal thresholds. The results of this analysis revealed that mGluR availability levels in several sensory and limbic brain structures were correlated with paw withdrawal thresholds in SNL animals (Table S1 and Table S2).

A negative interaction with the paw withdrawal thresholds was shown in (1) the striatum including the caudate putamen (contralateral to nerve injury) connected to the secondary somatosensory cortex (Fig. 1A), (2) the rostral striatum (contralateral to nerve injury) (Fig. 1B) connected to the insular cortex (Fig. 1C), and (3) the hippocampus (ipsilateral to nerve injury) (Fig. 1D) of SNL animals. This translates into greater mGluR5 availability in these regions, with more sensitive paw withdrawal behavior.

Conversely, a positive interaction with the paw withdrawal thresholds was shown in (1) the cingulate cortex (Fig. 2A), (2) the ipsilesional trunk region of the primary somatosensory cortex connected to the hippocampus (Fig. 2B), (3) the hypothalamus (Fig. 2C), (4) the contralesional trunk region, dysgranular zone, and barrel field of the primary somatosensory cortex (Fig. 2D), (5) the ipsilesional secondary somatosensory cortex (Fig. 2E), and (6) the ipsilesional hindlimb region of the primary somatosensory cortex (Fig. 2F) of SNL animals. This translates into a greater mGluR5 availability in these regions, with a less sensitive paw withdrawal behavior.

We used the region-of-interest (ROI) analysis to validate the results of the regression analysis. Based on the anatomical location of the significant clusters from the regression analysis, ROIs were set as the 0.5 mm radius sphere in each region (Fig. S2A and Table S3). The mGluR5 availability (BP_{ND}) of each ROI was extracted from the SNL group, and correlations between the paw withdrawal threshold and the individual BP_{ND} from each ROI were calculated (Fig. S3). These analyses confirmed significant correlations between the paw withdrawal threshold and mGluR5 BP_{ND} levels of each region (Figs. 1 and 2).

3.3. Correlation of mGluR5 availability levels between brain regions of SNL animals

As the brain regions were chosen on the basis of their interactions with functional outcome (i.e., paw withdrawal thresholds), the mGluR5 BP_{ND} in each region should have inter-subject correlations with each other. Indeed, the SNL group showed a high correlation between ROIs (Fig. 3A). There was a clear contrast between the clusters of positive and negative correlations in the matrix of r-value (Fig. 3A, left). These correlations were significant (P-value summary, Fig. 3A, right).

We aimed to assess whether this manifestation of inter-subject correlations is a feature specific to neuropathic pain group, rather than an intrinsic feature of the brain. To investigate this, the BP_{ND} of each ROI was extracted from the sham group (n = 10 rats) and their correlations were computed. The majority of the ROIs did not correlate with other regions, with only a few significant correlations in the matrices (Fig. 3B).

The significant regions that were correlated with paw withdrawal threshold in SNL group (Figs. 1 and 2) were not overlapped with the significant regions extracted by voxel-by-voxel two-sample *t*-test between SNL group and sham group (Chung et al., 2017). Therefore, it is suspected that the amount of mGluR5 availability levels in the regions of correlation would not be different between the SNL and sham groups. To confirm this, the BP_{ND} measurements of each ROI were compared using two-sample t-tests and F-tests. No significant differences were observed (Fig. S4). This suggests that the mGluR5 availability levels in these brain regions of the SNL group are in a normal range, despite the abnormal paw withdrawal threshold (Fig. S2, B and C).

These results demonstrate that mGluR5 availability levels in the sensory and limbic regions form distinct patterns in animals that underwent the neuropathic pain procedure, but not in controls. This raises the prospect that from a group-level perspective, mGluR5 BP_{ND} levels in these regions are 're-aligned' according to the paw withdrawal threshold following neuropathic pain. This might be due to the expressional and/or conformational change of the mGluR5 which affect tracer binding.

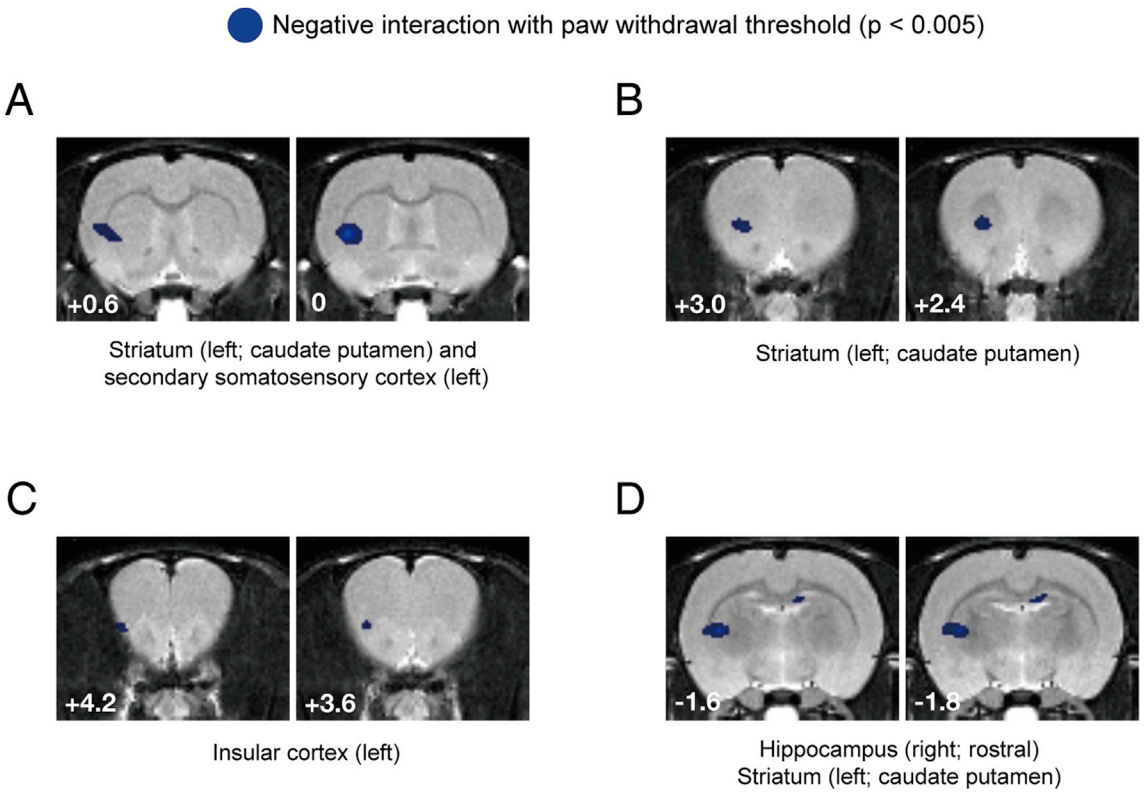

Fig. 1. Brain regions in which mGluR5 availability is negatively correlated to paw withdrawal threshold in the SNL group. This translates into higher mGluR5 availability in regions with a more sensitive right hind paw. A. A cluster including the left striatum (caudate putamen) connected to the secondary somatosensory cortex. B. A cluster in the left rostral striatum (caudate putamen). C. A cluster in the left insular cortex connected to a small portion of the orbitofrontal cortex. D. Clusters in the left striatum (caudate putamen) and the right hippocampus (CA3).

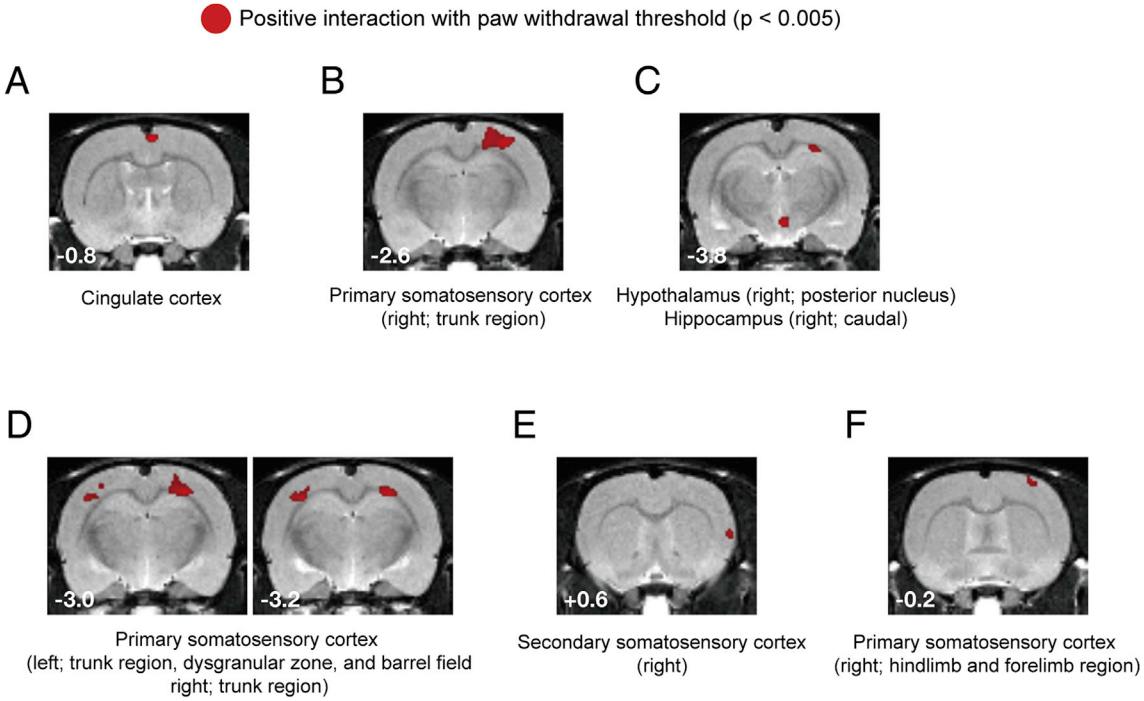

Fig. 2. Brain regions in which mGluR5 availability is positively correlated to the paw withdrawal threshold in the SNL group. This translates into higher mGluR5 availability in regions with a less sensitive right hind paw. A. A cluster in the cingulate cortex. B. A cluster in the right primary somatosensory cortex (trunk region). C. Clusters in the hypothalamus and the right hippocampus. D. Bilateral clusters in the primary somatosensory cortices. The cluster in the left primary somatosensory cortex includes the trunk region, dysgranular zone, and barrel field. The cluster in the right primary somatosensory cortex is largely constituted by the trunk region and connected to the right hippocampus. E. A cluster in the right secondary somatosensory cortex. F. A cluster in the right primary somatosensory cortex (hindlimb and forelimb regions).

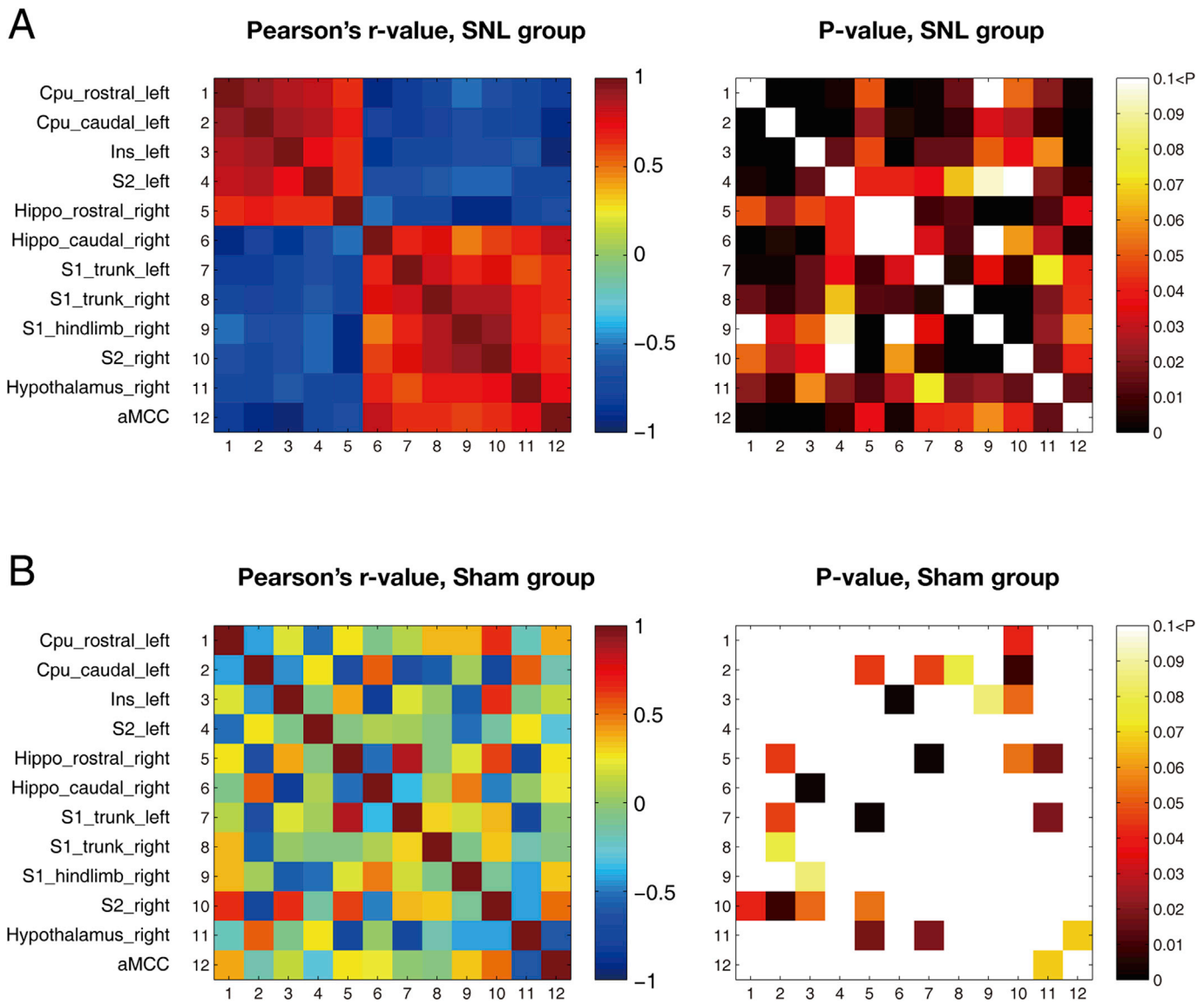

Fig. 3. The correlation coefficient between mGluR5 availability levels in the brain. mGluR5 availability levels in the corticolimbic areas show distinct correlation patterns in the SNL group only. A. Correlation coefficient matrices of the SNL group. A clear contrast between the clusters of positive and negative correlations was shown in the matrix of r-value (left). The significances of the correlations were further confirmed by their p-values (right). B. Correlation coefficient matrices of the sham group. The majority of the ROIs did not correlate with other regions, shown by small r-values (left). The majority of the p-values did not reach significance (right).

Consequently, the mGluR5 BP_{ND} levels of the ROIs show inter-subject correlations with each other in the neuropathic pain group. Notably, this re-alignment of mGluR5 BP_{ND} following neuropathic pain does not make the mGluR5 BP_{ND} levels in these regions exceed the physiological range.

3.4. *Decoding of the paw withdrawal threshold based on the mGluR5 patterns of neuropathic pain brain*

To assess the distribution range of the mGluR5 availability in each region, the BP_{ND} of each ROI was plotted by group (Fig. 4A and B). For normalization, all values were scaled in proportion to the average values of each region in the sham group (Fig. 4C and D). A representative template of the SNL group pattern was produced by regression of the normalized mGluR5 BP_{ND} levels to the paw withdrawal thresholds (Fig. 4E). Thus, each row of the template represents the pattern of normalized mGluR5 BP_{ND} levels in each brain regions of a hypothetical SNL rat that has a corresponding paw withdrawal threshold.

The degree of match of the original pattern with the regressed pattern was computed using Pearson's correlation coefficient method. The correlation coefficient between the pattern of each SNL rat (Fig. 4C) and the template (Fig. 4E) was calculated row-by-row, and the results of each rat were plotted in the columns (Fig. 5A and B). Thus, each column of the r-value and p-value matrices represents the result from an individual rat. As the template was produced from the SNL data, and the SNL data had been normalized in proportion to the average value, high correlations ($r > 0.5$) were shown on either side of the average level, depending on the original paw withdrawal threshold value of the subject. The matched patterns were shown by the range of the r-value (Fig. 5C). The range of $r > 0.5$ or $r > 75$ percentile was plotted to show the best-match between the mGluR5 pattern of the subject and the template, with the original paw withdrawal threshold of the subject assessed using the von Frey test (Fig. 5C). The results showed a good match between the original mGluR5 patterns of the SNL group animals and the patterns of the regressed template.

We questioned whether the mGluR5 patterns of the sham group

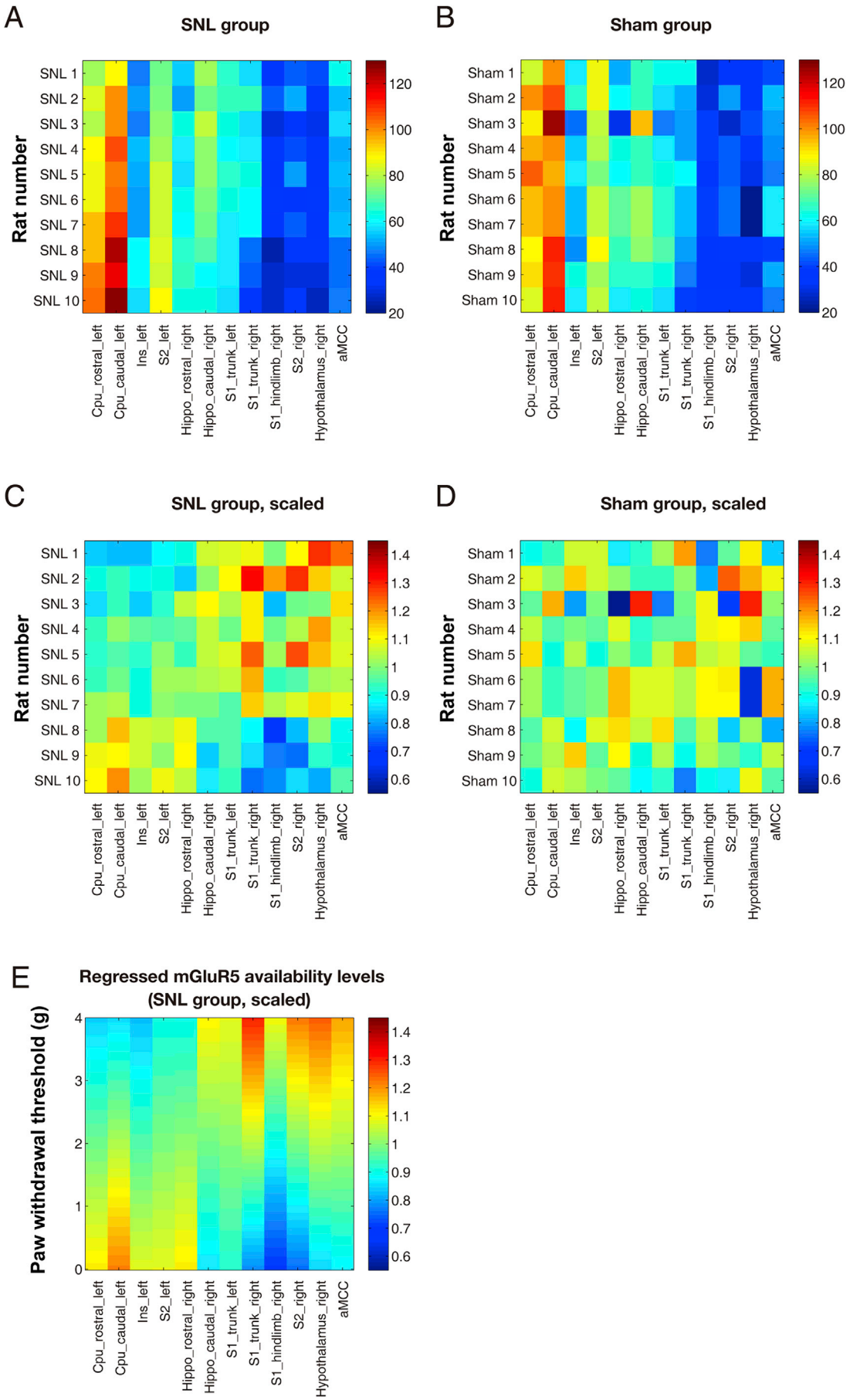

(caption on next page)

Fig. 4. mGluR5 availability in each ROI, and a representative template of mGluR5 pattern in the SNL group. A. The distribution range of mGluR5 availability in each ROI in the SNL group. B. The distribution range of mGluR5 availability in each ROI in the sham group. C. The mGluR5 availability levels in each region of SNL animals were scaled in proportion to the average values of each region in the sham group. D. Scaled mGluR5 availability levels in the sham group. E. A representative template of the SNL group pattern. Proportionally scaled mGluR5 availability levels of SNL rats were regressed to the paw withdrawal thresholds. Each row of the template represents the pattern of normalized mGluR5 availability in each brain region of a hypothetical SNL rat which has a corresponding paw withdrawal threshold.

animals matched the patterns of the SNL template by chance. To investigate this, the patterns of sham group animals (Fig. 4C) were compared to the SNL template (Fig. 4E) with the same method (Fig. 5D and E). To classify the image into SNL or sham group, the values of the columns were investigated in the matrices of both groups. The columns that contain the match satisfying $r > 0.5$ were predicted to be the SNL group. In the criteria, individual PET image could be predicted with 90% accuracy (100% sensitivity and 80% specificity). The accuracy reached 100% level when the cut-off r-value criterion was in the range of $0.555 < r < 0.754$ (Fig. 5F).

Further, we investigated the sensitivity of our method using a leave-one-subject-out cross-validation paradigm. In this method, the pattern data of one subject (a row in Fig. 4C) were left out, and the regressed template was created from data of the remaining nine subjects. Then data of the subject which had been left out were applied, to calculate the degree of match. This method was repeated subject-by-subject to predict all the paw withdrawal thresholds of SNL subjects. We observed that all the SNL subjects were correctly predicted by the method with 100% sensitivity, showing the existence of matches satisfying $r > 0.5$ in all of the SNL subjects (Fig. S5A and B). The high correlation range in this leave-one-out analysis was plotted with the paw withdrawal thresholds assessed using the von Frey test (Fig. S5C). We further performed an additional cross-validation. In this test, the PET image of one subject was left out, and the ROIs were selected based on data of the remaining nine subjects. Depending on the trials, 9 to 17 ROIs were selected. The data of the subject which had been left out were extracted, with the ROI set of the trial. The regressed template was created from data of the nine subjects, and then the data of the test sample were applied. Tests were repeated subject-by-subject (Fig. S5, D and E). In total tests, 80% sensitivity was obtained (Fig. S5F). The average specificity across 10 trials was 84%.

4. Discussion

Together, these results show that once a model template is established from the [11C] ABP688 PET images of neuropathic pain group, the status of the individual subject can be decoded using the regional patterns of the mGluR5 availability. We could predict which group the sample subject belonged to, and further estimate the extent of paw withdrawal threshold of SNL group animals using mGluR5 patterns. Regarding the

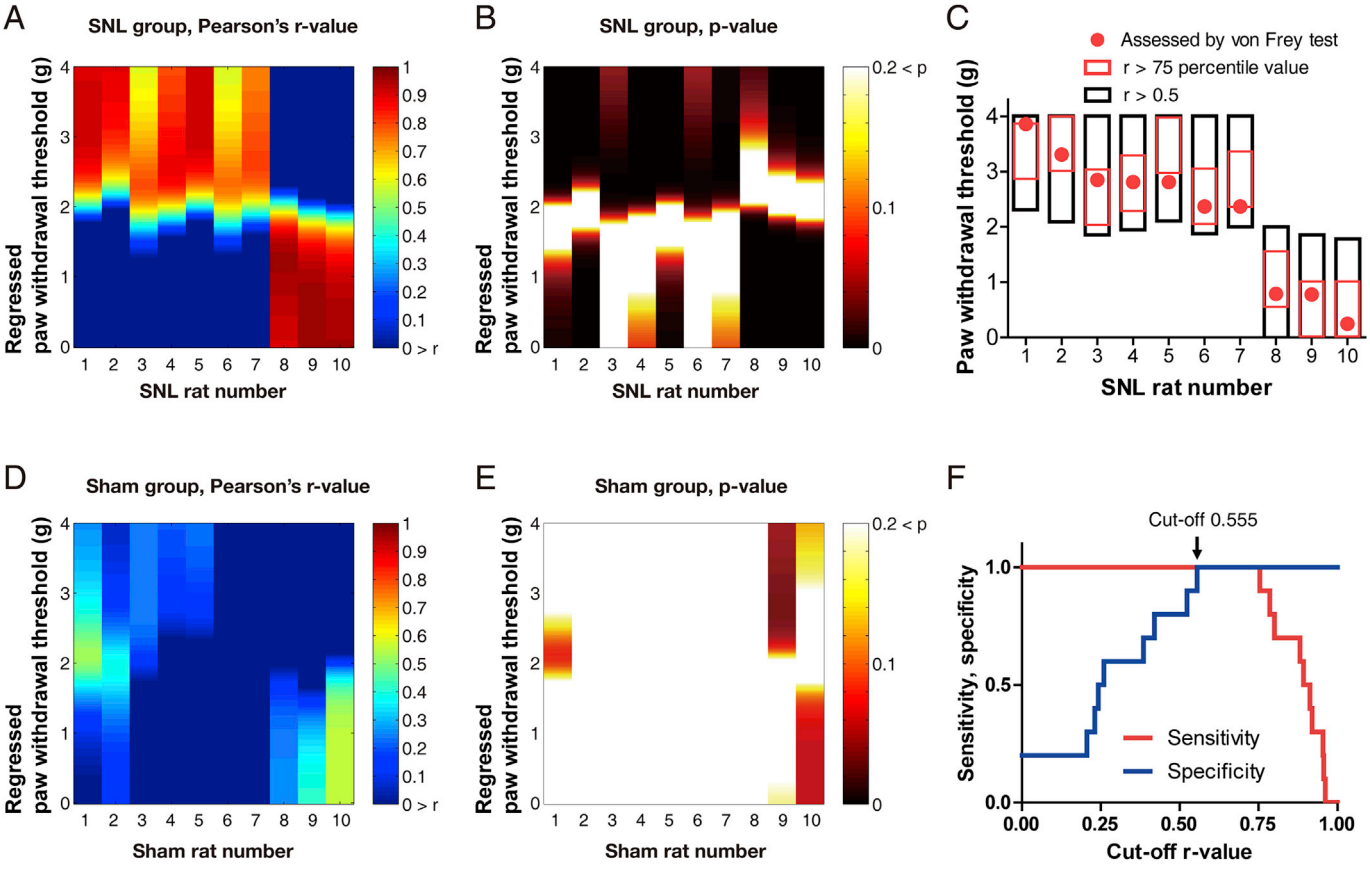

Fig. 5. The correlation between mGluR5 patterns of the regressed template and model animal predicts the presence and degree of neuropathic pain. A. The correlation coefficients between the pattern of each SNL rat and the regressed SNL template. Each column represents the result from an individual rat. mGluR5 values from SNL rats showed high correlation with values of the SNL template. B. The p-value matrix of SNL group. C. Best-match ranges. The match ranges of the pattern correlation successfully predicted the original paw withdrawal threshold of the subject. D. The correlation coefficients between the pattern of each sham rat and the regressed SNL template. The mGluR5 values of sham rats showed poor correlations with the values of the SNL template. E. The p-value matrix of the sham group. F. Receiver-operating characteristic curve. The subject which contained an r-value above the cut-off level was predicted as the SNL group. The subject could be predicted whether it belonged to the SNL or sham group with 100% accuracy when the cut-off level was in the range of $0.555 < r < 0.754$.

significant role of mGluR5 in regulating neuronal excitability, we propose that the mGluR5 "fingerprints" imprinted within the sensory and limbic structures of neuropathic pain brain reflect the functional cross-talk between sensory perception and behavioral coping.

4.1. Variation in pain behavior

Variation in paw withdrawal threshold in neuropathic pain animals (Fig. S1) might involve the degree of peripheral hypersensitivity, amplified aversive perception of the nervous system, and altered response strategy for coping behavior following nociception. With the analysis of [11C] ABP688-PET images, we demonstrated the brain regions in which the mGluR5 availability is correlated with the paw withdrawal threshold of neuropathic pain model animals. The brain regions are mainly constituted of sensory and limbic structures which are known to participate in sensory processing, decision making, and coping behaviors. Although it is difficult to interpret whether these correlations reflect passive change of mGluR5 following peripheral pain amplification or intrinsic regional function of mGluR5 as a determinant responsible for the execution of pain behavior, the critical role of the corticolimbic system in pain processing and avoidance behavior is in agreement with previous studies (Baliki et al., 2014; Boeke et al., 2017; Bravo-Rivera et al., 2015; Cardinal et al., 2002; Fardo et al., 2017; Navratilova and Porreca, 2014; Orenius et al., 2017).

4.2. The limbic structures

We found that the striatal (caudate-putamen) mGluR5 is negatively correlated (Fig. 1A and B and D), whereas the somatosensory mGluR5 is positively correlated (Fig. 2, B, D, E and F), with paw withdrawal thresholds (with the exception of a negative correlation of the left secondary somatosensory cortex, Fig. 1A). Thus, the higher availability levels of striatal mGluR5 or the lower availability levels of somatosensory mGluR5 are connected to a more sensitive paw withdrawal behavior to tactile stimulus. The hippocampus showed both a positive and negative correlation depending on subregion. Strikingly, these brain areas overlap with the regions identified by a previous analysis of fMRI-based connectivity. Baliki et al. (2014) demonstrated that the hippocampus shows increased functional connectivity to the striatum and decreased functional connectivity to the sensorimotor cortex in neuropathic pain animals, and that these changes correlate with the degree of nerve injury-induced reduction of paw withdrawal thresholds. According to that study, the hippocampus-striatum connectivity is negatively correlated, whereas the hippocampus-sensorimotor cortex connectivity is positively correlated, with the paw withdrawal thresholds. Thus, the higher level of hippocampus-striatum connectivity or the lower level of hippocampus-sensorimotor connectivity of neuropathic pain animals is connected to a more sensitive paw withdrawal behavior for tactile stimulus. They proposed that the interconnection between these brain regions plays a significant role in the manifestation of neuropathic pain. The results from our PET analysis support this view, and further implicate mGluR5 as a determinant of connectivity between these brain regions.

Besides the hippocampus and the striatum, significant clusters of mGluR5 were also located in other limbic structures such as the cingulate cortex (Fig. 2A) and the hypothalamus (Fig. 2C). In the case of the cingulate cortex (Fig. 2A), the anterior-posterior range of the significant cluster was -0.4 mm ~ -1.4 mm from bregma, located in the anterior part of the midcingulate cortex (aMCC) (Vogt and Paxinos, 2014). This region is involved in error detection (conflict monitoring) and cognitive control (Parvaz et al., 2014; Procyk et al., 2014), and engaged in evaluating the necessity of behavioral adaption (Wessel et al., 2012). Our data suggest that mGluR5 in this region affects decision making related to the execution of behavioral coping, and thus correlates with von Frey stimuli-induced avoidance behavior. In the case of the hypothalamus, a significant mGluR5 cluster was located on the right side of the posterior nucleus (Fig. 2C). Regarding the sympathetic dependency of SNL-induced neuropathic pain (Kim et al., 1997), the positive correlation of a significant cluster suggests that mGluR5 in the posterior nucleus of hypothalamus suppresses withdrawal behavior via control of autonomic nervous tone.

4.3. The somatosensory cortices

One unexpected result was the significant correlation of paw withdrawal threshold with the hindlimb region of ipsilateral, but not contralateral, primary somatosensory cortex. SNL rats were subjected to the right L5 SNL surgery, and therefore the withdrawal threshold of the right hind paw was assessed and used for regression analysis. Although many significant clusters in other subregions of primary somatosensory cortices were located bilaterally (Fig. 2D), correlation with hindlimb region was shown only in the right (ipsilateral to nerve injury) primary somatosensory cortex (Fig. 2F). The mGluR5 availability in the hindlimb region of the right primary somatosensory cortex was positively correlated with the paw withdrawal threshold, which indicates that the higher mGluR5 availability was, the less withdrawal behavior of the right hind paw was elicited. This might be explained by interhemispheric inhibition of the contralateral corresponding hindlimb area by the ipsilateral primary somatosensory cortex (Clarey et al., 1996; Hlushchuk and Hari, 2006). Unilateral somatosensory cortex participates in interhemispheric inhibition of the contralateral sensorimotor cortex, and thus influences sensory discrimination of transcallosal somatosensory cortex and aids in the motor control (Iwata et al., 2016; Lei and Perez, 2017; Zapallow et al., 2013). In addition, the transcallosal communication between bilateral corresponding somatosensory area is known to be involved in the mirror-image pain (Ishikawa et al., 2018). The nerve injury-induced pain would reciprocally interact with the mGluR5-mediated excitatory and inhibitory influences in the ipsilesional and contralesional somatosensory cortices (Ishikawa et al., 2018; Kim et al., 2016).

In the case of the secondary somatosensory cortex, the left and right secondary somatosensory cortices showed an opposite direction in terms of the correlation to paw withdrawal threshold (Figs. 1A and 2E), further supporting the idea above. The positive correlation of right secondary somatosensory cortex, and the negative correlation of left secondary somatosensory cortex, with paw withdrawal threshold, translates into a less sensitive hind paw with higher mGluR5 availability in the right secondary somatosensory cortex and/or lower mGluR5 availability in the left secondary somatosensory cortex. This suggests that among the bilateral somatosensory cortices, only mGluR5 in the left secondary somatosensory cortex might exacerbate tactile hypersensitivity of the right hind paw. In contrast, mGluR5 availability levels in the right secondary somatosensory cortex, trunk region of the bilateral primary somatosensory cortices, and hindlimb region of the right primary somatosensory cortex might mitigate the hypersensitivity of the right hind paw.

4.4. The pain processing in the corticolimbic circuits

In the previous research, we compared the mGluR5 levels in the brains of SNL surgery animals and sham surgery animals using voxel-by-voxel two-sample t-tests (Chung et al., 2017). The resulting significant ROI clusters did not overlap in a coordinated space with the results of current regression study, although some clusters were located within the same anatomical structures (e.g., insular cortex, somatosensory cortices, and striatum). This disagreement between clusters with SNL-induced mGluR5 alteration and clusters which correlate to the withdrawal thresholds implies that the mGluR5 levels of each neural circuits represent separate stages of pain processing. According to the dynamic causal model of a recent study (Roy et al., 2014), a system of interconnected regions including the caudate putamen, hippocampus, and ventromedial prefrontal cortex encodes expectancies of behavioral outcome (expected pain and avoidance value), and activity of the putamen is most closely related to the expected value. In this causality model, the expected value signals from the putamen and the prediction error signals calculated in

the midbrain periaqueductal gray are then transmitted to orbitofrontal cortex and aMCC, updating the value in the dorsomedial prefrontal cortex. While that study was conducted in humans and the model was produced based on fMRI experiments, participating brain regions revealed in that model largely overlap with ROIs extracted from our analyses. We interpret the aberrant levels of mGluR5 in affected brain regions (such as the prelimbic subregion of the medial prefrontal cortex) in the SNL animals of our previous study (Chung et al., 2017) as maladaptation in the chronic pain state, which affects updating appraisal of internal perception. In contrast, mGluR5 levels in the brain regions of behavioral correlation in the current regression analysis were in a physiological range (Fig. S2), and thus their correlation with withdrawal threshold might reflect the normal physiological mGluR5 function of the system which affects encoding behavioral strategies (Roy et al., 2014) or regulating the sensory perception. We propose that mGluR5 in the significant brain regions affects the withdrawal threshold of nerve-injured subjects via functional regulation of sensory processing and behavioral coding in the somatosensory and limbic circuitry.

4.5. The advancements

In the other previous study of ours, we distinguished neuropathic pain animals and control animals using brain images acquired with [18F] fluorodeoxyglucose – PET (Kim et al., 2014). Using multivariate pattern analysis, we could successfully predict which group (SNL or sham) the subjects belonged to. In the current study, we could predict the extent of the pain severity, and calculate to what extent they are similar to the reference patterns, in addition to predicting whether the subject is pain positive or pain negative. There are unmet needs for the objective pain assessment for the human patients, and we suggest that the mGluR5 pattern analysis we described here could be a useful tool in the clinic as a measure of the pain status.

4.6. The limitations

The estimation of the mGluR5 availability in each brain regions could be affected by biases resulted from various factors. As the spatial resolution of the PET image is poor and some of the brain areas we are handling are very small, biases could be introduced by the partial volume effects. In addition, the calculation of the BP_{ND} in our research might be affected by small amounts of mGluR5 expression in the deep cerebellar nuclei, as we did not strictly exclude the deep cerebellar nuclei region when we set the reference ROI in the cerebellum for the simplified reference tissue model. However, we believe that this possible bias would not affect the main results of the current study, as the cerebellar mGluR5 level is extremely low and the binding of the ABP688 is negligible in the cerebellum compared to the cerebral structures we are dealing with (Ametamey et al., 2007; Elmenhorst et al., 2010). The other factor we could not control for during the study design is a diurnal fluctuation of the mGluR5 in the brain (David Elmenhorst, 2016; DeLorenzo et al., 2017). In our research, the PET scans were performed mostly during the daytime (11:18–13:20) in 14 rats ($n = 7$ per each group). However, 6 rats ($n = 3$ per each group) experienced PET scan during the late afternoon and early evening (16:58–18:04). The bias might be caused by the time when the scan was performed, although we could not find a significant interaction between the scan start time and the mGluR5 availability levels in our data (Fig. S6).

5. Conclusion

In conclusion, we report the correlation between brain mGluR5 availability levels and nerve injury-induced reduction of paw withdrawal threshold in a rodent model of neuropathic pain. A correlation was observed in the somatosensory cortices and limbic structures of the brain, emphasizing a critical role of mGluR5 in these regions with respect to neuropathic pain perception and resulting reactive behavior. Owing to the interactions between sensory perception and behavioral coping, regional mGluR5 availability levels form distinct patterns in the brain of neuropathic pain subjects. Using the distinct "fingerprints" of mGluR5 availability, the status of individuals could be precisely predicted. Together with previous studies (Chung et al., 2017; Kim et al., 2016), the current research reveals a significant involvement of brain mGluR5 in the manifestation of neuropathic pain, and identifies brain circuits that may be further studied to clarify the mechanisms underlying altered sensory perception and behavioral coping in neuropathic pain subjects.

Funding

This work was supported by grants from the National Research Foundation of Korea (2012R1A5A2A44671346, 2015H1A2A1034977, 2017M3C7A1029611, 2018R1A6A3A11045706, and BK21 Plus Project), and Seoul National University Hospital Research Fund (320150250). The funding sources had no involvement in study design, in the collection, analysis and interpretation of data, in the writing of the manuscript, and in the decision to submit the article for publication.

Financial disclosures

The authors declare that there is no conflict of interest.

Acknowledgments

GC conceived and designed the study, processed and analyzed data, and wrote the manuscript. CYK contributed to the processing of data. SK contributed to the conception of the study. The data used in this study are from our previous research (Chung et al., 2017).

Appendix A. Supplementary data

Supplementary data related to this article can be found at https://doi.org/10.1016/j.neuroimage.2018.07.016.

References

Ametamey, S.M., Treyer, V., Streffer, J., Wyss, M.T., Schmidt, M., Blagoev, M., Hintermann, S., Auberson, Y., Gasparini, F., Fischer, U.C., Buck, A., 2007. Human PET studies of metabotropic glutamate receptor subtype 5 with ^{11}C-ABP688. J. Nucl. Med. 48, 247–252.

Baliki, M.N., Apkarian, A.V., 2015. Nociception, pain, negative moods, and behavior selection. Neuron 87, 474–491. https://doi.org/10.1016/j.neuron.2015.06.005.

Baliki, M.N., Chang, P.C., Baria, A.T., Centeno, M.V., Apkarian, A.V., 2014. Resting-sate functional reorganization of the rat limbic system following neuropathic injury. Sci. Rep. 4, 6186. https://doi.org/10.1038/srep06186.

Baliki, M.N., Petre, B., Torbey, S., Herrmann, K.M., Huang, L., Schnitzer, T.J., Fields, H.L., Apkarian, A.V., 2012. Corticostriatal functional connectivity predicts transition to chronic back pain. Nat. Neurosci. 15, 1117–1119. https://doi.org/10.1038/nn.3153.

Baron, R., Förster, M., Binder, A., 2012. Subgrouping of patients with neuropathic pain according to pain-related sensory abnormalities: a first step to a stratified treatment approach. Lancet Neurol. 11, 999–1005. https://doi.org/10.1016/S1474-4422(12)70189-8.

Boeke, E.A., Moscarello, J.M., LeDoux, J.E., Phelps, E.A., Hartley, C.A., 2017. Active avoidance: neural mechanisms and attenuation of pavlovian conditioned responding. J. Neurosci. 37, 4808–4818. https://doi.org/10.1523/JNEUROSCI.3261-16.2017.

Bouhassira, D., Attal, N., 2016. Translational neuropathic pain research: a clinical perspective. Neuroscience 338, 27–35. https://doi.org/10.1016/j.neuroscience.2016.03.029.

Bravo-Rivera, C., Roman-Ortiz, C., Montesinos-Cartagena, M., Quirk, G.J., 2015. Persistent active avoidance correlates with activity in prelimbic cortex and ventral striatum. Front. Behav. Neurosci. 9, 184. https://doi.org/10.3389/fnbeh.2015.00184.

Brett, M., Anton, J.-L.L., Valabregue, R., Poline, J.-B., 2002. Region of interest analysis using an SPM toolbox. In: Abstract Presented at the 8th International Conference on Functional Mapping of the Human Brain, June 2-6, 2002, Sendai, Japan. Neuroimage 16, Abstract 497. https://doi.org/10.1016/S1053-8119(02)90010-8.

Cardinal, R.N., Parkinson, J.A., Hall, J., Everitt, B.J., 2002. Emotion and motivation: the role of the amygdala, ventral striatum, and prefrontal cortex. Neurosci. Biobehav. Rev. 26, 321–352.

Chaplan, S.R., Bach, F.W., Pogrel, J.W., Chung, J.M., Yaksh, T.L., 1994. Quantitative assessment of tactile allodynia in the rat paw. J. Neurosci. Meth. 53, 55–63. https://doi.org/10.1016/0165-0270(94)90144-9.

Chung, G., Kim, C.Y., Yun, Y.-C., Yoon, S.H., Kim, M.-H., Kim, Y.K., Kim, S.J., 2017. Upregulation of prefrontal metabotropic glutamate receptor 5 mediates neuropathic pain and negative mood symptoms after spinal nerve injury in rats. Sci. Rep. 7, 9743. https://doi.org/10.1038/s41598-017-09991-8.

Clarey, J.C., Tweedale, R., Calford, M.B., 1996. Interhemispheric modulation of somatosensory receptive fields: evidence for plasticity in primary somatosensory cortex. Cerebr. Cortex 6, 196–206. https://doi.org/10.1093/cercor/6.2.196.

Coffeen, U., Ortega-Legaspi, J.M., de Gortari, P., Simón-Arceo, K., Jaimes, O., Amaya, M.I., Pellicer, F., 2010. Inflammatory nociception diminishes dopamine release and increases dopamine D2 receptor mRNA in the Rat's insular cortex. Mol. Pain 6, 1744–8069. https://doi.org/10.1186/1744-8069-6-75, 6–75.

David Elmenhorst, C., 2016. Circadian Variation of Metabotropic Glutamate Receptor 5 Availability in the Rat Brain. https://doi.org/10.1111/jsr.12432.

Davis, D.A., Ghantous, M.E., Farmer, M.A., Baria, A.T., Apkarian, A.V., 2016. Identifying brain nociceptive information transmission in patients with chronic somatic pain. PAIN Reports 1, e575. https://doi.org/10.1097/PR9.0000000000000575.

DeLorenzo, C., Gallezot, J.-D., Gardus, J., Yang, J., Planeta, B., Nabulsi, N., Ogden, R.T., Labaree, D.C., Huang, Y.H., Mann, J.J., Gasparini, F., Lin, X., Javitch, J.A., Parsey, R.V., Carson, R.E., Esterlis, I., 2017. In vivo variation in same-day estimates of metabotropic glutamate receptor subtype 5 binding using [^{11} C]ABP688 and [^{18} F] FPEB. J. Cerebr. Blood Flow Metabol. 37, 2716–2727. https://doi.org/10.1177/0271678X16673646.

Detloff, M.R., Clark, L.M., Hutchinson, K.J., Kloos, A.D., Fisher, L.C., Basso, D.M., 2010. Validity of acute and chronic tactile sensory testing after spinal cord injury in rats. Exp. Neurol. 225, 366–376. https://doi.org/10.1016/j.expneurol.2010.07.009.

Dixon, W.J., 1965. The up-and-down method for small samples. J. Am. Stat. Assoc. 60, 967–978. https://doi.org/10.1080/01621459.1965.10480843.

Elmenhorst, D., Minuzzi, L., Aliaga, A., Rowley, J., Massarweh, G., Diksic, M., Bauer, A., Rosa-Neto, P., 2010. In vivo and in vitro validation of reference tissue models for the mGluR 5 ligand [^{11}C]ABP688. J. Cerebr. Blood Flow Metabol. 30, 1538–1549. https://doi.org/10.1038/jcbfm.2010.65.

Fardo, F., Auksztulewicz, R., Allen, M., Dietz, M.J., Roepstorff, A., Friston, K.J., 2017. Expectation violation and attention to pain jointly modulate neural gain in somatosensory cortex. Neuroimage 153, 109–121. https://doi.org/10.1016/j.neuroimage.2017.03.041.

Felice, M., De Sanoja, R., Wang, R., Vera-portocarrero, L., Oyarzo, J., King, T., Ossipov, M.H., Vanderah, T.W., Lai, J., Dussor, G.O., Fields, H.L., Price, T.J., Porreca, F., 2011. Engagement of descending inhibition from the rostral ventromedial medulla protects against chronic neuropathic pain. Pain 152, 2701–2709. https://doi.org/10.1016/j.pain.2011.06.008.

Fitzgerald, M., McKelvey, R., 2016. Nerve injury and neuropathic pain — a question of age. Exp. Neurol. 275, 296–302. https://doi.org/10.1016/j.expneurol.2015.07.013.

Hlushchuk, Y., Hari, R., 2006. Transient suppression of ipsilateral primary somatosensory cortex during tactile finger stimulation. J. Neurosci. 26, 5819–5824. https://doi.org/10.1523/JNEUROSCI.5536-05.2006.

Kim, S.H., Chung, J.M., 1992. An experimental model for peripheral neuropathy produced by segmental spinal nerve ligation in the rat. Pain 50, 355–363. https://doi.org/10.1016/0304-3959(92)90041-9.

Hogan, Q., Sapunar, D., Modric-Jednacak, K., McCallum, J.B., 2004. Detection of neuropathic pain in a rat model of peripheral nerve injury. Anesthesiology 101, 476–487. https://doi.org/10.1097/00000542-200408000-00030.

Hu, L., Iannetti, G.D., 2016. Painful issues in pain prediction. Trends Neurosci. 39, 212–220. https://doi.org/10.1016/j.tins.2016.01.004.

Ishikawa, T., Eto, K., Kim, S.K., Wake, H., Takeda, I., Horiuchi, H., Moorhouse, A.J., Ishibashi, H., Nabekura, J., 2018. Cortical astrocytes prime the induction of spine plasticity and mirror image pain. Pain 1. https://doi.org/10.1097/j.pain.0000000000001248.

Iwata, Y., Jono, Y., Mizusawa, H., Kinoshita, A., Hiraoka, K., 2016. Interhemispheric inhibition induced by transcranial magnetic stimulation over primary sensory cortex. Front. Hum. Neurosci. 10, 438. https://doi.org/10.3389/fnhum.2016.00438.

Kim, C.-E., Kim, Y.K., Chung, G., Im, H.J., Lee, D.S., Kim, J., Kim, S.J., 2014. Identifying neuropathic pain using ^{18}F-FDG micro-PET: a multivariate pattern analysis. Neuroimage 86, 311–316. https://doi.org/10.1016/j.neuroimage.2013.10.001.

Kim, K.J., Yoon, Y.W., Chung, J.M., 1997. Comparison of three rodent neuropathic pain models. Exp. Brain Res. 113, 200–206. https://doi.org/10.1007/BF02450318.

Kim, S.K., Hayashi, H., Ishikawa, T., Shibata, K., Shigetomi, E., Shinozaki, Y., Inada, H., Roh, S.E., Kim, S.J., Lee, G., Bae, H., Moorhouse, A.J., Mikoshiba, K., Fukazawa, Y., Koizumi, S., Nabekura, J., 2016. Cortical astrocytes rewire somatosensory cortical circuits for peripheral neuropathic pain. J. Clin. Invest. 126, 1983–1997. https://doi.org/10.1172/JCI82859.

Kras, J.V., Dong, L., Winkelstein, B.A., 2014. Increased Interleukin-1α and prostaglandin E2 expression in the spinal cord at 1 Day after painful facet joint injury. Spine 39, 207–212. https://doi.org/10.1097/BRS.0000000000000107.

Lei, Y., Perez, M.A., 2017. Cortical contributions to sensory gating in the ipsilateral somatosensory cortex during voluntary activity. J. Physiol. https://doi.org/10.1113/JP274504.

Litaudon, P., Bouillot, C., Zimmer, L., Costes, N., Ravel, N., 2017. Activity in the rat olfactory cortex is correlated with behavioral response to odor: a microPET study. Brain Struct. Funct. 222, 577–586. https://doi.org/10.1007/s00429-016-1235-8.

Massart, R., Dymov, S., Millecamps, M., Suderman, M., Gregoire, S., Koenigs, K., Alvarado, S., Tajerian, M., Stone, L.S., Szyf, M., 2016. Overlapping signatures of chronic pain in the DNA methylation landscape of prefrontal cortex and peripheral T cells. Sci. Rep. 6, 19615. https://doi.org/10.1038/srep19615.

Navratilova, E., Porreca, F., 2014. Reward and motivation in pain and pain relief. Nat. Neurosci. 17, 1304–1312. https://doi.org/10.1038/nn.3811.

Orenius, T.I., Raij, T.T., Nuortimo, A., Näätänen, P., Lipsanen, J., Karlsson, H., 2017. The interaction of emotion and pain in the insula and secondary somatosensory cortex. Neuroscience 349, 185–194. https://doi.org/10.1016/j.neuroscience.2017.02.047.

Ossipov, M.H., Lai, J., Malan, T.P., Porreca, F., 2000. Spinal and supraspinal mechanisms of neuropathic pain. Ann. N. Y. Acad. Sci. 909, 12–24.

Parvaz, M.A., Maloney, T., Moeller, S.J., Malaker, P., Konova, A.B., Alia-Klein, N., Goldstein, R.Z., 2014. Multimodal evidence of regional midcingulate gray matter volume underlying conflict monitoring. NeuroImage Clin 5, 10–18. https://doi.org/10.1016/j.nicl.2014.05.011.

Procyk, E., Wilson, C.R.E., Stoll, F.M., Faraut, M.C.M., Petrides, M., Amiez, C., 2014. Midcingulate motor map and feedback detection: converging data from humans and monkeys. Cerebr. Cortex 26. https://doi.org/10.1093/cercor/bhu213 bhu213.

Roy, M., Shohamy, D., Daw, N., Jepma, M., Wimmer, G.E., Wager, T.D., 2014. Representation of aversive prediction errors in the human periaqueductal gray. Nat. Neurosci. 17, 1607–1612. https://doi.org/10.1038/nn.3832.

Saadé, N.E., Amin, H.A., Chalouhi, S., Baki, S.A., Jabbur, S.J., Atweh, S.F., 2006. Spinal pathways involved in supraspinal modulation of neuropathic manifestations in rats. Pain 126, 280–293. https://doi.org/10.1016/j.pain.2006.07.010.

Schweinhardt, P., Fransson, P., Olson, L., Spenger, C., Andersson, J.L.R., 2003. A template for spatial normalisation of MR images of the rat brain. J. Neurosci. Meth. 129, 105–113. https://doi.org/10.1016/S0165-0270(03)00192-4.

Singleton, J.R., 2005. Evaluation and treatment of painful peripheral polyneuropathy. Semin. Neurol. 25, 185–195. https://doi.org/10.1055/s-2005-871327.

Tran, J., Dorstyn, D.S., Burke, A.L.J., 2016. Psychosocial aspects of spinal cord injury pain: a meta-analysis. Spinal Cord 54, 640–648. https://doi.org/10.1038/sc.2016.66.

Vachon-Presseau, E., Tétreault, P., Petre, B., Huang, L., Berger, S.E., Torbey, S., Baria, A.T., Mansour, A.R., Hashmi, J.A., Griffith, J.W., Comasco, E., Schnitzer, T.J., Baliki, M.N., Apkarian, A.V., 2016. Corticolimbic anatomical characteristics predetermine risk for chronic pain. Brain 139, 1958–1970. https://doi.org/10.1093/brain/aww100.

van Wilgen, C.P., Keizer, D., 2012. The sensitization model to explain how chronic pain exists without tissue damage. Pain Manag. Nurs. 13, 60–65. https://doi.org/10.1016/j.pmn.2010.03.001.

Vase, L., Skyt, I., Hall, K.T., 2016. Placebo, nocebo, and neuropathic pain. Pain 157, S98–S105. https://doi.org/10.1097/j.pain.0000000000000445.

Vogt, B.A., Paxinos, G., 2014. Cytoarchitecture of mouse and rat cingulate cortex with human homologies. Brain Struct. Funct. 219, 185–192. https://doi.org/10.1007/s00429-012-0493-3.

von Hehn, C.A., Baron, R., Woolf, C.J., 2012. Deconstructing the neuropathic pain phenotype to reveal neural mechanisms. Neuron 73, 638–652. https://doi.org/10.1016/j.neuron.2012.02.008.

Wager, T.D., Atlas, L.Y., Lindquist, M.A., Roy, M., Woo, C.-W., Kross, E., 2013. An fMRI-based neurologic signature of physical pain. N. Engl. J. Med. 368, 1388–1397. https://doi.org/10.1056/NEJMoa1204471.

Wei, X., Sun, Y., Luo, F., 2017. Impaired spinal glucocorticoid receptor signaling contributes to the attenuating effect of depression on mechanical allodynia and thermal hyperalgesia in rats with neuropathic pain. Front. Cell. Neurosci. 11, 145. https://doi.org/10.3389/fncel.2017.00145.

Wessel, J.R., Danielmeier, C., Morton, J.B., Ullsperger, M., 2012. Surprise and error: common neuronal architecture for the processing of errors and novelty. J. Neurosci. 32, 7528–7537. https://doi.org/10.1523/JNEUROSCI.6352-11.2012.

Yalcin, I., Barthas, F., Barrot, M., 2014. Emotional consequences of neuropathic pain: insight from preclinical studies. Neurosci. Biobehav. Rev. 47, 154–164. https://doi.org/10.1016/j.neubiorev.2014.08.002.

Zapallow, C.M., Jacobs, M.F., Lee, K.G.H., Asmussen, M.J., Tsang, P., Nelson, A.J., 2013. Continuous theta-burst stimulation over the primary somatosensory cortex modulates interhemispheric inhibition. Neuroreport 24, 394–398. https://doi.org/10.1097/WNR.0b013e32836131ca.